Novel Detectors for Passive Radar Sensing with I/Q Imbalance and Additive Distortion

Junqiu Wang, Yunfei Chen, *Senior Member, IEEE*

***Abstract*—Passive radar has been recognized as one of the most attractive and promising approaches to solving the critical challenge of spectrum scarcity. However, the ubiquitous hardware impairment (HWI) might severely degrade the passive radar's performance. This article develops maximum likelihood estimate algorithms considering I/Q imbalance (IQI) and additive distortion (AD) to propose the generalized likelihood ratio test (GLRT) based detectors. For single-target cases, the novel GLRT detectors correspond to different knowledge levels of the transmitted signals and channel state information. Then, the single-target scenarios are extended to the two-target case to investigate the effects of transmitter-receiver distance, bistatic range and range resolution brought by the interfering target. Specifically, we propose the HWI mitigation algorithm to approximate and simplify the complex GLRT expressions due to the interfering target, thereby counteracting the effects of IQI and AD. Finally, simulation results demonstrate that both amplitude mismatch and phase mismatch have degrading impact on the overall detection probability of single-target passive radar, and the two-target detector has a very high range resolution compared with classical works in DVB-T. Also, the range resolution is proven to be robust to HWI.**

***Index Terms*—Additive distortion, GLRT detectors, I/Q imbalance, passive radar, range limit, range resolution.**

I. Introduction

Spectral scarcity has been a significant technical challenge in wireless communications. There have been several effective solutions in recent decades to alleviate this problem. One approach is to utilize the unlicensed industrial, scientific, and medical (ISM) bands. Near-field communications are such a technology to use the ISM, thus mitigating the challenge of spectrum scarcity [1]. To address the mismatch between optimal beamformers at the center frequency and their poor performance at distinct radio frequencies within the wide bandwidth for millimeter wave and terahertz communications using massive phased arrays, a low-complexity technique InFocus was proposed to mitigate the misfocus effect in the near-field system [2]. Different transmit antenna structures for near-field signalling, including fully-digital architectures, hybrid phase shifter-based precoders, and the emerging dynamic metasurface antenna architecture for massive multiple-input multiple-output (MIMO) arrays were studied to explore the potential of feasible beams [3]. Long-term evolution (LTE) access to the unlicensed spectrum is also helpful in solving spectrum scarcity [4]. The performance of coexistence between LTE and Wi-Fi systems was evaluated by focusing on a system-level simulation analysis to assess the network performance in an office scenario [5]. The computing offloading problem for private industrial Internet-of-Things (IoT) enabled by LTE over unlicensed spectrum technology was investigated to figure out the channel availability and task arrivals via the proposed constrained deep Q-learning based task scheduling algorithm with provable convergence [6]. Another approach is dynamic spectrum access which mainly employs the cognitive radio (CR) to dynamically find unused spectrum bands and temporarily utilize them for secondary users [7]. In [8], the authors boosted energy efficiency for data transmission in licensed channels via a two-way information exchange dynamic spectrum sensing algorithm in clustered CR-IoT networks. A cache-enabled unmanned aerial vehicles cooperation scheme in the CR network was proposed to reduce the redundant traffic load and enhance the transmission capability of CR network in the work of [9]. Besides, there is also a choice to use the spectrum bands at extremely high frequencies like visible light communications (VLC). For example, a new field of view geometry-based single bounce model for VLC channels was proposed to mitigate the effects of channel distortions [10]. The authors in [11] developed a comprehensive VLC channel modeling and characterization based on ray tracing which was capable of receiving channel impulse responses for any nonideal sources.

Different from the above solutions, joint radar and communications (JRC) attempts to achieve the spectrum sharing of radar system bands that fall into the S-band (2-4 GHz) and C-band (4-8 GHz) with communications systems according to three categories: codesign, coexistence and cooperation [12]. On the one hand, the networking of multiple radars requires complex communications techniques to improve the overall radar performance [13]. On the other hand, the communications systems could be aided by radar to discover a neighbor more quickly [13]. Therefore, JRC has been under intensive investigation and becomes one of the most successful methods to solve spectrum scarcity. In particular, codesign achieves the spectrum sharing by jointly designing a dual-functional radar communications (DFRC) system. Reference [14] proposed an integrated signal model that simultaneously communicated with downlink users and detected radar targets by optimizing the transmit beamforming to match the desired radar beampattern while satisfying the communications performance requirements. An optimization problem of the weighted summation of radar signal and communications signal was formulated, and solved by semidefinite relaxation algorithm based on zero-forcing technique in [15]. To cancel the interference of active waveforms from radars, two algorithms were

Junqiu Wang is with the School of Engineering, University of Warwick, Coventry, UK, CV4 7AL. e-mail:Qiuqiu.Wang@warwick.ac.uk.

Yunfei Chen is with the Department of Engineering, University of Durham, Durham, UK, DH1 3LE. e-mail:Yunfei.Chen@durham.ac.uk.

proposed to jointly estimate the waveform and demodulate the received data by implementing an iterative process [16]. The authors of [17] investigated the effect of interference from an unaltered radar system on the performance of both single-carrier and multi-carrier communications systems, then they proposed the complex-valued constellation design problems to either maximize the transmission rate or minimize the error rate. The cooperative spectrum sharing and joint sampling scheme between a MIMO-matrix completion radar and a communications system were devised to reduce the radar receiver's effective interference power further without compromising the capacity and transmit power to the communications system below a certain level [18]. In [19], a hybrid active passive MIMO radar network was designed by employing target returns from both the radar transmitters and communications transmitters, while the communications system could extract useful information not only from communications receiver but also from radar echo signals from the target.

The interest in passive radar is excellent among all the cooperative JRC regimes. Passive radar can utilize the radio frequency (RF) signals from a communications system as the illuminator of opportunity (IO) to detect potential targets in a bistatic passive setting. In this setting, a typical passive radar system often receives the signal transmitted directly from the IO in the reference channel (RC) and the signal reflected by the potential target in the surveillance channel (SC). Thus, passive radar requires no emission of radar signals and avoids revealing the position of its own sensor [20]. Due to its complete covertness and passiveness, frequency allocation is not required to deploy the passive radar receiver. Therefore, the passive radar is able to operate in densely populated areas with a lot of IO signals at various frequencies [20]. Besides, this passive setting has some extra advantages over conventional radars, including lower cost, smaller space and much higher portability [21]. Therefore, it has become an interesting research topic for JRC designs.

There have been a number of works on passive radar. For example, the normalized cross ambiguity function (NCAF) was proposed to combine information contaminated by the Gaussian noise from both RC and SC, and the cumulative distribution function of NCAF was derived in [22]. Direct-path interference in multistatic passive radar was considered using a generalized likelihood ratio test (GLRT) detector in [23]. The extensive cancellation algorithm was modified to a sliding window version subject to limitations, and its counteracting effect against these limitations was demonstrated by estimating the filter coefficients in [24]. In [25], a proper reference signal was reconstructed by analyzing the basis expansion model for the channel and using antenna diversity and channel estimation to alleviate the severe distortion of digital video broadcasting-terrestrial (DVB-T) orthogonal frequency division multiplexing (OFDM) signals in an airborne passive radar system. In [26], the authors considered the performance variability for different signal-to-noise ratios (SNRs) in RC and SC, and proposed several GLRT detectors to achieve significant performance improvement over the conventional cross-correlation detectors. In [27], the analytical expressions of the cross-correlation detector's false alarm probability and detection probability were given to explore the extent to which the interference and noise shall be suppressed, and the superiority of cross-correlation detectors over matched filter detectors was shown. Direct signal interference mitigation was examined to identify the primary factors affecting interference suppression for various spectrally and spatially diverse digital television (DTV) waveforms under realistic situations in [28]. The multistatic passive radar based on single-antenna DTV processing was proposed to analyze the detection range in the drone detection scenario [29].

Most of the works mentioned above have assumed that the transceiver hardware is ideal. However, communications devices are known to suffer from hardware impairment (HWI), such as power amplifier nonlinearity, phase noise and in-phase and quadrature imbalance (IQI). These HWI will affect the system performance by distorting image signals, causing phase and amplitude mismatch and raising the noise floor [30]. Several works have examined the effect of HWI on communications systems. For example, the analytical expression for the outage probability (OP) at the amplify-and-forward dual-hop relay suffering from IQI was derived over non-identical and independent Nakagami-m fading channels [31]. In [32], the authors derived the analytical symbol error rate for MIMO OFDM systems over Rayleigh channels. They showed that receive (RX) IQI has a more considerable impact than transport (TX) IQI and that extra RX antennas could mitigate RX IQI. Full-duplex cooperative non-orthogonal multiple access relaying systems suffering from imperfect successive interference cancellation and IQI were studied regarding the ergodic sum rate and the OP [33].

Besides IQI, additive distortion (AD) is another common type of HWI. The analytical expression for OP and the optimal beamforming for a dual-hop MIMO amplify-and-forward relay were studied with AD in [34]. Considering both IQI and AD direct-conversion radio, closed-form expressions for the false alarm and detection probabilities were derived and extended to cognitive radio networks in [35]. The improper Gaussian signaling (IGS) scheme was compared with the traditional proper Gaussian signaling scheme in terms of achievable rate and OP, and IGS was found to counteract AD efficiently [36].

All of the above works have shown that HWI is an important factor limiting communications performances. However, they have not considered HWI in a passive radar setting that uses communications signals. There have been works on HWI for active radar systems. For example, a 160 GHz frequency-modulated continuous-wave (FMCW) radar was investigated with a HWI mitigation method in [37]. In [38], a parametric radar model considering chirp-sequence and HWI was proposed. In [39], the signal-to-distortion-plus-noise ratio and range-Doppler sensitivity with constant false alarm rate were studied for a 77 GHz FMCW automotive radar with both IQI and phase noise. Nevertheless, active radars and passive radars are very different in terms of hardware, set-up and IO. Thus, these results cannot be used for passive radars.

Motivated by the above observations, our work focuses on novel detectors considering IQI and AD in passive radar sensing. The major contributions of this article are summarized as follows:

1) We present a practical passive radar framework to solve the spectrum scarcity. This system model considers the HWI of IQI and AD at both the TX (IO) and the passive radar's RX.
2) The detector design problem is formulated as a parameter estimation problem for GLRT. For the single-target cases, the closed analytical forms of four novel detectors are derived via maximum likelihood estimate method corresponding to four scenarios with different knowledge levels of the transmitted signals and channel state information.
3) The single-target GLRT problem is extended to the two-target GLRT problem to investigate the performance of operation range limit and range resolution in the presence of an interfering target. To tackle this issue, we propose the HWI mitigation algorithm to approximate and simplify the GLRT formulas, which avoids processing the complicated HWI terms.
4) Numerical results show that IQI has a significant degrading impact on the detection probability of the single-target passive radar detectors. Especially the amplitude mismatch has more impact than the phase mismatch. Also, the proposed HWI mitigation algorithm is proven to provide stable range resolution regardless of IQI.

The remainder of this paper is organized as follows. Section II presents the passive radar model with HWI. Section III derives the new detectors in various realistic single-target scenarios. Section IV gives the detector with an interfering target to investigate the range limit and range resolution. Section V provides simulation results of the impact of HWI on the performance of the proposed detectors. Finally, conclusions are made in Section VI.

Notations: The Italic letter denotes a scalar and the lower case boldface letter represents a vector. $CN(\cdot,\cdot)$ denotes a complex Gaussian random variable. $\mathrm{E}(\cdot)$ represents the expectation operation. $\mathrm{Re}(\cdot)$ and $\mathrm{Im}(\cdot)$ represent the real part and the imaginary part of a complex number, respectively.

II. System model

Similar to that in [26], it is assumed that both the IO and the passive radar receiver have a single antenna. The RC is the direct-path from the IO to the passive radar receiver. The SC is the path where the transmitted signal is reflected by the object to be detected at the passive radar receiver. Assume that the transmitted information signal is $s(t)$ with $\mathrm{E}(|s(t)|^2) = P$. For the i-th transmitted sample with a sampling frequency f_s at the time instants $t = i/f_s, i = 1, ..., I$, we use subscript i to represent it as s_i. This sample firstly suffers from the IQI at the transmitter to become

$$s_{t,i} = G_1 s_i + G_2 s_i^*, i = 1, 2, \ldots, \tag{1}$$

where $G_1 = \frac{1+a_t e^{-i\phi_t}}{2}$, $G_2 = 1 - {G_1}^*$, a_t and ϕ_t are the amplitude and phase mismatch at the transmitter due to the IQI, respectively. Then the additive distortion d_i due to the imperfect power amplification is added to $s_{t,i}$ as

$$s_{d,i} = s_{t,i} + d_i = G_1 s_i + G_2 s_i^* + d_i. \tag{2}$$

TABLE I
RELEVANT SYMBOL NOTATIONS

Notation	Definition
G_1, G_2	IQI coefficient at the IO transmitter
K_1, K_2	IQI coefficient at the passive radar receiver
$a_t = a_r = a$	Amplitude mismatch of the transceiver
$\phi_t = \phi_r = \phi$	Phase mismatch of the transceiver
h_r	Reference channel gain
h_s	Surveillance channel gain
$h_{s,1}$	Surveillance channel gain of desired target
$h_{s,2}$	Surveillance channel gain of interfering target
P	Signal transmission power
s	Transmitted signal
d	Additive noise
w_r	Additive white Gaussian noise in reference channel
w_s	Additive white Gaussian noise in surveillance channel
L	Transmitter-receiver distance
R	Bistatic range of the desired target
δ_R	Bistatic range difference between two targets
f_s	Sampling frequency
y_r	The final received signal of reference channel
y_s	The final received signal of surveillance channel

At the illuminator of opportunity's transmitter, there is an additive distortion $d_{t,i}$. Also, there is an additive distortion $d_{r,i}$ at the passive radar's receiver. By considering the aggregate effect of the $d_{t,i}$ and $d_{r,i}$, it is equivalent to be an additive distortion d_i at the transmitter. Therefore, d_i has been modelled as complex Gaussian with $d_i \sim \mathcal{CN}(0, \left(\sigma_t^2 + \sigma_r^2\right) P')$ where $P' = \mathrm{E}(|s_{t,i}|^2)$, σ_t^2 and σ_r^2 are the variances of the additive distortion at the transmitter and the receiver, respectively, in all previous works. This is motivated by the central limit theorem from various RF stages and the details of the explanation can be found in [40], [41]. Under different hypotheses, one has the received signal $x_{r,i}$ from the RC and the received signal $x_{s,i}$ from the SC as

$$H_0 : \begin{cases} x_{\mathrm{r,i}} = h_r s_{d,i} + w_{r,i} \\ x_{\mathrm{s,i}} = w_{s,i} \end{cases}, H_1 : \begin{cases} x_{\mathrm{r,i}} = h_r s_{d,i} + w_{r,i} \\ x_{\mathrm{s,i}} = h_s s_{d,i} + w_{s,i} \end{cases}, \tag{3}$$

where h_r and h_s are the channel gains in the RC and SC, respectively, $w_{r,i}$ and $w_{s,i}$ are the additive white Gaussian noise (AWGN) in the RC and SC, respectively. They are independent and identically distributed complex Gaussian random variables with $\mathcal{CN}(0, \sigma_w^2)$. Similarly, $x_{r,i}$ and $x_{s,i}$ also suffer from the IQI at the receiver with $K_1 = \frac{1+a_r e^{i\phi_r}}{2}$, $K_2 = 1 - {K_1}^*$, where a_r and ϕ_r are the amplitude and phase mismatch at the receiver, respectively. In our work, we assume that $a_t = a_r = a$ and $\phi_t = \phi_r = \phi$ for convenience. Therefore, the received signals after considering all HWI are

$$\begin{cases} y_{\mathrm{r,i}} = K_1 x_{r,i} + K_2 x_{r,i}^* \\ y_{\mathrm{s,i}} = K_1 x_{s,i} + K_2 x_{s,i}^*. \end{cases} \tag{4}$$

Substituting (2) and (3) into (4), one has

$$\begin{aligned} H_0 : \begin{cases} y_{r,i} = a_r s_i + b_r s_i^* + z_{r,i} \\ y_{s,i} = K_1 w_{s,i} + K_2 w_{s,i}^* \end{cases}, \\ H_1 : \begin{cases} y_{r,i} = a_r s_i + b_r s_i^* + z_{r,i} \\ y_{s,i} = a_s s_i + b_s s_i^* + z_{s,i} \end{cases}, \end{aligned} \tag{5}$$

where

$$\begin{cases} a_r = K_1 G_1 h_r + K_2 G_2^* h_r^* \\ b_r = K_1 G_2 h_r + K_2 G_1^* h_r^* \\ z_{r,i} = K_1 h_r d_i + K_2 h_r^* d_i^* + K_1 w_{r,i} + K_2 w_{r,i}^* \end{cases}, \quad \begin{cases} a_s = K_1 G_1 h_s + K_2 G_2^* h_s^* \\ b_s = K_1 G_2 h_s + K_2 G_1^* h_s^* \\ z_{s,i} = K_1 h_s d_i + K_2 h_s^* d_i^* + K_1 w_{s,i} + K_2 w_{s,i}^*. \end{cases} \tag{6}$$

In the next section, we will propose the corresponding detectors for various situations.

III. New Detectors

For the detection at the passive radar receiver, we take I received samples as given in (5). At the IO transmitter, the transmitted information signal sample vector is $\boldsymbol{s} = [s_1, s_2, ..., s_I]$. At the passive radar receiver, the received signal sample vectors are $\boldsymbol{y}_r = [y_{r,1}, y_{r,2}, ..., y_{r,I}]$ and $\boldsymbol{y}_s = [y_{s,1}, y_{s,2}, ..., y_{s,I}]$ in RC and SC, respectively. For a specific sample $y_{r,i}$ in $\boldsymbol{y}_r$ and $y_{s,i}$ in $\boldsymbol{y}_s$, the joint likelihood function of $(y_{r,i}, y_{s,i})$ under hypothesis H_0 is $l_{H_0,i}(y_{r,i}, y_{s,i}) = l_{r,H_0}(y_{r,i}) \cdot l_{s,H_0}(y_{s,i})$ where l_{r,H_0} and l_{s,H_0} are the likelihood functions of $y_{r,i}$ and $y_{s,i}$ under H_0, respectively. Similarly, under hypothesis H_1, the joint likelihood function of $(y_{r,i}, y_{s,i})$ is $l_{H_1,i}(y_{r,i}, y_{s,i}) = l_{r,H_1}(y_{r,i}) \cdot l_{s,H_1}(y_{s,i})$, where l_{r,H_1} and l_{s,H_1} are the likelihood function of $y_{s,i}$ under H_1. Note that $y_{r,i}$ is the same for both H_0 and H_1. Thus, let $l_{r,H_0}(y_{r,i}) = l_{r,H_1}(y_{r,i}) = l_r(y_{r,i})$ in the following. Due to the introduction of I/Q imbalance coefficients K_1 and K_2, $K_1 w_{r,i} + K_2 w_{r,i}^*$ and $K_1 h_r d_i + K_2 h_r^* d_i^*$ are improper Gaussian random variables [40]. Therefore, $z_{r,i}$ is an improper Gaussian variable, and so is $z_{s,i}$. Using the probability density function of the improper Gaussian variable in [42], one has

$$\begin{cases} l_r(y_{r,i}) = \frac{1}{\pi a \cos\phi\left(|h_r|^2\sigma_d^2+\sigma_w^2\right)} e^{-\frac{A_{ri}}{a^2\cos^2\phi\left(|h_r|^2\sigma_d^2+\sigma_w^2\right)}} \\ l_{s,H_1}(y_{s,i}) = \frac{1}{\pi a \cos\phi\left(|h_s|^2\sigma_d^2+\sigma_w^2\right)} e^{-\frac{A_{si,H_1}}{a^2\cos^2\phi\left(|h_s|^2\sigma_d^2+\sigma_w^2\right)}} \\ l_{s,H_0}(y_{s,i}) = \frac{1}{\pi a \cos\phi\left(|h_s|^2\sigma_d^2+\sigma_w^2\right)} e^{-\frac{A_{si,H_0}}{a^2\cos^2\phi\left(|h_s|^2\sigma_d^2+\sigma_w^2\right)}} \end{cases}, \tag{7}$$

where

$$\begin{aligned} A_{ri} &= a^2 \mathrm{Re}^2(y_{r,i} - a_r s_i - b_r s_i^*) + \mathrm{Im}^2(y_{r,i} - a_r s_i - b_r s_i^*) \\ &\quad - 2a(\sin\phi)\,\mathrm{Re}(y_{r,i} - a_r s_i - b_r s_i^*)\,\mathrm{Im}(y_{r,i} - a_r s_i - b_r s_i^*), \end{aligned} \tag{8}$$

$$\begin{aligned} A_{si,H_1} &= a^2 \mathrm{Re}^2(y_{s,i} - a_s s_i - b_s s_i^*) \\ &\quad - 2a(\sin\phi)\,\mathrm{Re}(y_{s,i} - a_s s_i - b_s s_i^*)\,\mathrm{Im}(y_{s,i} - a_s s_i - b_s s_i^*) \\ &\quad + \mathrm{Im}^2(y_{s,i} - a_s s_i - b_s s_i^*), \end{aligned} \tag{9}$$

and

$$\begin{aligned} A_{si,H_0} &= a^2 \mathrm{Re}^2(y_{s,i}) + \mathrm{Im}^2(y_{s,i}) \\ &\quad - 2a(\sin\phi)\,\mathrm{Re}(y_{s,i})\,\mathrm{Im}(y_{s,i}). \end{aligned} \tag{10}$$

Then, one has

$$\begin{cases} l_{H_0}(\boldsymbol{y}_r, \boldsymbol{y}_s) = \prod_{i=1}^{I} l_{H_0,i}(y_{r,i}, y_{s,i}) \\ l_{H_1}(\boldsymbol{y}_r, \boldsymbol{y}_s) = \prod_{i=1}^{I} l_{H_1,i}(y_{r,i}, y_{s,i}) \end{cases}, \tag{11}$$

where $l_{H_0}(\boldsymbol{y}_r, \boldsymbol{y}_s)$ and $l_{H_1}(\boldsymbol{y}_r, \boldsymbol{y}_s)$ are the joint likelihood functions under H_0 and H_1, respectively. According to the Neyman–Pearson criterion, the detection is performed by taking the ratio of the likelihood function $l_{H_1}(\boldsymbol{y}_r, \boldsymbol{y}_s)$ over the likelihood function $l_{H_0}(\boldsymbol{y}_r, \boldsymbol{y}_s)$ with an appropriate detection threshold as

$$R(\boldsymbol{y}_r, \boldsymbol{y}_r) = R = \frac{l_{H_1}(\boldsymbol{y}_r, \boldsymbol{y}_s)}{l_{H_0}(\boldsymbol{y}_r, \boldsymbol{y}_s)} \gtrless_{H_0}^{H_1} \gamma, \tag{12}$$

where γ denotes the detection threshold. To further simplify the detection, one can take the logarithm of (11) as

$$\begin{aligned} \ln R(\boldsymbol{y}_r, \boldsymbol{y}_r) &= \ln R \\ &= \ln l_{H_1}(\boldsymbol{y}_r, \boldsymbol{y}_s) - \ln l_{H_0}(\boldsymbol{y}_r, \boldsymbol{y}_s) \\ &\gtrless_{H_0}^{H_1} \ln\gamma. \end{aligned} \tag{13}$$

From (5) and (6), one sees that $l_{H_0}(\boldsymbol{y}_r, \boldsymbol{y}_s)$ is dependent of h_r and $\boldsymbol{s}$ while $l_{H_1}(\boldsymbol{y}_r, \boldsymbol{y}_s)$ is dependent of h_r, h_s and $\boldsymbol{s}$, where h_r, h_s and $\boldsymbol{s}$ might be unknown and need to be estimated. We denote the MLEs of h_r, h_s and $\boldsymbol{s}$ under H_1 as $\hat{h}_{r,H_1}$, $\hat{h}_{s,H_1}$ and $\hat{\boldsymbol{s}}_{H_1}$, respectively. One has

$$\begin{aligned} ln_{H_1} &= \ln l_{H_1}(\boldsymbol{y}_r, \boldsymbol{y}_s | \hat{h}_{r,H_1}, \hat{h}_{s,H_1}, \hat{\boldsymbol{s}}_{H_1}) \\ &= -I\ln\left(|\hat{h}_{r,H_1}|^2\sigma_d^2 + \sigma_w^2\right) - I\ln\left(|\hat{h}_{s,H_1}|^2\sigma_d^2 + \sigma_w^2\right) \\ &\quad - \frac{\left(|\hat{h}_{s,H_1}|^2\sigma_d^2 + \sigma_w^2\right)\sum_{i=1}^{I}\hat{A}_{ri,H_1}}{a^2\cos^2\phi\left(|\hat{h}_{r,H_1}|^2\sigma_d^2 + \sigma_w^2\right)\left(|\hat{h}_{s,H_1}|^2\sigma_d^2 + \sigma_w^2\right)} \\ &\quad - \frac{\left(|\hat{h}_{r,H_1}|^2\sigma_d^2 + \sigma_w^2\right)\sum_{i=1}^{I}\hat{A}_{si,H_1}}{a^2\cos^2\phi\left(|\hat{h}_{r,H_1}|^2\sigma_d^2 + \sigma_w^2\right)\left(|\hat{h}_{s,H_1}|^2\sigma_d^2 + \sigma_w^2\right)} \\ &\quad - 2I\ln(\pi a\cos\phi), \end{aligned} \tag{14}$$

where $\hat{A}_{ri,H_1}$ and $\hat{A}_{si,H_1}$ are the estimated value of A_{ri} and A_{si,H_1} under H_1, respectively. They are functions of $\hat{h}_{r,H_1}$, $\hat{h}_{s,H_1}$ and $\hat{\boldsymbol{s}}_{H_1}$. Similarly, by denoting the MLEs of h_r and $\boldsymbol{s}$ under H_0 as $\hat{h}_{r,H_0}$ and $\hat{\boldsymbol{s}}_{H_0}$, respectively, one has

$$\begin{aligned} ln_{H_0} &= \ln l_{H_0}(\boldsymbol{y}_r, \boldsymbol{y}_s | \hat{h}_{r,H_0}, \hat{\boldsymbol{s}}_{H_0}) \\ &= -I\ln\left(|\hat{h}_{r,H_0}|^2\sigma_d^2 + \sigma_w^2\right) - I\ln\sigma_w^2 \\ &\quad - \frac{\sum_{i=1}^{I}\hat{A}_{ri,H_0}}{a^2\cos^2\phi\left(|\hat{h}_{r,H_0}|^2\sigma_d^2 + \sigma_w^2\right)} - \frac{\sum_{i=1}^{I}A_{si,H_0}}{a^2\cos^2\phi\,(\sigma_w^2)} \\ &\quad - 2I\ln(\pi a\cos\phi), \end{aligned} \tag{15}$$

where $\hat{A}_{ri,H_0}$ is the estimated value of A_{ri} under H_0. It is a function of $\hat{h}_{r,H_0}$ and $\hat{\boldsymbol{s}}_{H_0}$. Different detectors will be derived based on (14) and (15) in the following subsections.

A. Coherent detector

In this detector, we assume that h_r, h_s and $\boldsymbol{s}$ are all known so that $\hat{h}_{r,H_1} = \hat{h}_{r,H_0} = h_r$, $\hat{h}_{s,H_1} = h_s$ and $\hat{\boldsymbol{s}}_{H_1} = \hat{\boldsymbol{s}}_{H_0} = \boldsymbol{s}$. This is the case for integrated radar-communications designs when the radar function and the communications function use the same device to share information between them. Let $h_r =$

$|h_r|e^{i\theta_r}$, $h_s = |h_s|e^{i\theta_s}$ and $\theta = \theta_r - \theta_s$. To get the desired detector, we firstly tackle the terms of A_{ri} and A_{si,H_1} in (8) and (9) by substituting $G_1 = \frac{1+ae^{-i\phi}}{2}$, $G_2 = 1 - {G_1}^*$, $K_1 = \frac{1+ae^{i\phi}}{2}$ and $K_2 = 1 - {K_1}^*$ to get

$$\begin{aligned} A_{ri} &= a^2|h_r|^2\cos^2(\phi)B_i(s_i) + a|h_r|\cos(\phi)C_{r,i}(\theta_r) \\ &+ a^2 {y_{r,i}^R}^2 - 2a\sin(\phi)y_{r,i}^R y_{r,i}^I + {y_{r,i}^I}^2, \end{aligned} \tag{16}$$

and

$$\begin{aligned} A_{si,H_1} &= a^2|h_s|^2\cos^2(\phi)B_i(s_i) + a|h_s|\cos(\phi)C_{s,i}(\theta_s) \\ &+ a^2 {y_{s,i}^R}^2 - 2a\sin(\phi)y_{s,i}^R y_{s,i}^I + {y_{s,i}^I}^2, \end{aligned} \tag{17}$$

where

$$\begin{aligned} B_i(s_i) &= -a^2\sin(2\phi)s_i^R s_i^I + a^2\cos^2(\phi)(s_i^I)^2 \\ &+ (s_i^R)^2\left(a^2\sin^2\phi + 1\right), \end{aligned} \tag{18}$$

$$\begin{aligned} C_{r,i}(\theta_r) &= 2s_i^R y_{r,i}^I\left(a\sin(\phi)\cos(\theta_r) - \sin(\theta_r)\right) \\ &+ 2a\cos(\phi)s_i^I\left(a y_{r,i}^R\sin(\theta_r+\phi) - \cos(\theta_r)y_{r,i}^I\right) \\ &+ s_i^R a y_{r,i}^R\left(a\cos(\theta_r+2\phi) - a\cos(\theta_r) - 2\cos(\theta_r+\phi)\right), \end{aligned} \tag{19}$$

and

$$\begin{aligned} C_{s,i}(\theta_s) &= 2s_i^R y_{s,i}^I\left(a\sin(\phi)\cos(\theta_s) - \sin(\theta_s)\right) \\ &+ 2a\cos(\phi)s_i^I\left(a y_{s,i}^R\sin(\theta_s+\phi) - \cos(\theta_s)y_{s,i}^I\right) \\ &+ s_i^R a y_{s,i}^R\left(a\cos(\theta_s+2\phi) - a\cos(\theta_s) - 2\cos(\theta_s+\phi)\right), \end{aligned} \tag{20}$$

with $y_{s,i}^R = \mathrm{Re}(y_{s,i})$, $y_{r,i}^R = \mathrm{Re}(y_{r,i})$, $y_{s,i}^I = \mathrm{Im}(y_{s,i})$ and $y_{r,i}^I = \mathrm{Im}(y_{r,i})$. Denote $A_r = \sum_{i=1}^{I} A_{ri}$ and $A_{s,H_1} = \sum_{i=1}^{I} A_{si,H_1}$, then one has

$$\begin{aligned} A_r &= a^2|h_r|^2\cos^2(\phi)B(\boldsymbol{s}) + a|h_r|\cos(\phi)C_r(\theta_r) \\ &+ a^2\sum_{i=1}^{I}{y_{r,i}^R}^2 - 2a\sin(\phi)\sum_{i=1}^{I}y_{r,i}^R y_{r,i}^I + \sum_{i=1}^{I}{y_{r,i}^I}^2, \end{aligned} \tag{21}$$

and

$$\begin{aligned} A_{s,H_1} &= a^2|h_s|^2\cos^2(\phi)B(\boldsymbol{s}) + a|h_s|\cos(\phi)C_s(\theta_s) \\ &+ \sum_{i=1}^{I}A_{si,H_0}, \end{aligned} \tag{22}$$

where $B(\boldsymbol{s}) = \sum_{i=1}^{I}B_i(s_i)$, $C_r(\theta_r) = \sum_{i=1}^{I}C_{r,i}(\theta_r)$ and $C_s(\theta_s) = \sum_{i=1}^{I}C_{s,i}(\theta_s)$. Using (20)-(22), one has

$$\begin{aligned} ln_{H_1} &= -I\ln\left(|h_r|^2\sigma_d^2 + \sigma_w^2\right) - I\ln\left(|h_s|^2\sigma_d^2 + \sigma_w^2\right) \\ &- \frac{a^2|h_r|^2\cos^2(\phi)B(\boldsymbol{s}) + a|h_r|\cos(\phi)C_r(\theta_r) + a^2\sum_{i=1}^{I}{y_{r,i}^R}^2}{a^2\cos^2\phi\left(|h_r|^2\sigma_d^2 + \sigma_w^2\right)} \\ &- \frac{a^2|h_s|^2\cos^2(\phi)B(\boldsymbol{s}) + a|h_s|\cos(\phi)C_s(\theta_s) + \sum_{i=1}^{I}A_{si,H_0}}{a^2\cos^2\phi\left(|h_s|^2\sigma_d^2 + \sigma_w^2\right)} \\ &- \frac{-2a\sin(\phi)\sum_{i=1}^{I}y_{r,i}^R y_{r,i}^I + \sum_{i=1}^{I}{y_{r,i}^I}^2}{a^2\cos^2\phi\left(|h_r|^2\sigma_d^2 + \sigma_w^2\right)} - 2I\ln(\pi a\cos\phi), \end{aligned} \tag{23}$$

$$\begin{aligned} ln_{H_0} &= -I\ln\left(|h_r|^2\sigma_d^2 + \sigma_w^2\right) - 2I\ln(\pi a\cos\phi) - I\ln\sigma_w^2 \\ &- \frac{a^2|h_r|^2\cos^2(\phi)B(\boldsymbol{s}) + a|h_r|\cos(\phi)C_r(\theta_r)}{a^2\cos^2\phi\left(|h_r|^2\sigma_d^2 + \sigma_w^2\right)} \\ &- \frac{a^2\sum_{i=1}^{I}{y_{r,i}^R}^2 - 2a\sin(\phi)\sum_{i=1}^{I}y_{r,i}^R y_{r,i}^I + \sum_{i=1}^{I}{y_{r,i}^I}^2}{a^2\cos^2\phi\left(|h_r|^2\sigma_d^2 + \sigma_w^2\right)} \\ &- \frac{\sum_{i=1}^{I}A_{si,H_0}}{a^2\cos^2\phi\left(\sigma_w^2\right)}. \end{aligned} \tag{24}$$

Therefore, (13) becomes

$$\begin{aligned} \Lambda_0 &= ln_{H_1} - ln_{H_0} \\ &= -I\ln\left(|h_s|^2\sigma_d^2 + \sigma_w^2\right) + I\ln\sigma_w^2 + \frac{\sum_{i=1}^{I}A_{si,H_0}}{a^2\cos^2\phi\left(\sigma_w^2\right)} \\ &- \frac{a^2|h_s|^2\cos^2(\phi)B(\boldsymbol{s}) + a|h_s|\cos(\phi)C_s(\theta_s) + \sum_{i=1}^{I}A_{si,H_0}}{a^2\cos^2(\phi)\left(|h_s|^2\sigma_d^2 + \sigma_w^2\right)} \\ &\gtrless_{H_0}^{H_1} T_0, \end{aligned} \tag{25}$$

where the proposed coherent detector Λ_0 is denoted as the CH-GLRT ('CH' means 'coherent') detector and the detection threshold T_0 will be determined by the predetermined false alarm probability.

B. GLRT with known $\boldsymbol{s}$

In this case, we only know the transmitted information vector $\boldsymbol{s}$ while h_r and h_s are unknown, so that $\hat{\boldsymbol{s}}_{H_1} = \hat{\boldsymbol{s}}_{H_0} = \boldsymbol{s}$, while h_s and h_r can be independently estimated under H_1 and H_0, respectively. Using (15) and (21), one has

$$\begin{aligned} f_0(|h_r|,\theta_r) &= \frac{a^2|h_r|^2\cos^2(\phi)B(\boldsymbol{s}) + a|h_r|\cos(\phi)C_r(\theta_r)}{a^2\cos^2\phi\left(|h_r|^2\sigma_d^2 + \sigma_w^2\right)} \\ &+ \frac{a^2\sum_{i=1}^{I}{y_{r,i}^R}^2 - 2a\sin(\phi)\sum_{i=1}^{I}y_{r,i}^R y_{r,i}^I + \sum_{i=1}^{I}{y_{r,i}^I}^2}{a^2\cos^2\phi\left(|h_r|^2\sigma_d^2 + \sigma_w^2\right)} \\ &+ I\ln\left(|h_r|^2\sigma_d^2 + \sigma_w^2\right), \end{aligned} \tag{26}$$

with which the MLEs of θ_r as $\hat{\theta}_{r,H_0}$ and $|h_r|$ as $|\widetilde{h}_{r,H_0}|$ under H_0 are obtained, respectively. Similarly, the MLEs $\hat{\theta}_{s,H_1}$ and $|\widetilde{h}_{s,H_1}|$ under H_1 can also be obtained. Thus, one has

$$\begin{aligned} \Lambda_1 &= ln_{H_1} - ln_{H_0} \\ &= -I\ln\left(|\widetilde{h}_{s,H_1}|^2\sigma_d^2 + \sigma_w^2\right) + I\ln\sigma_w^2 + \frac{\sum_{i=1}^{I}A_{si,H_0}}{a^2\cos^2\phi\left(\sigma_w^2\right)} \\ &- \frac{a^2|\widetilde{h}_{s,H_1}|^2\cos^2(\phi)B(\boldsymbol{s}) - a|\widetilde{h}_{s,H_1}|\cos(\phi)D_s(\boldsymbol{s})}{a^2\cos^2\phi\left(|\widetilde{h}_{s,H_1}|^2\sigma_d^2 + \sigma_w^2\right)} \\ &- \frac{\sum_{i=1}^{I}A_{si,H_0}}{a^2\cos^2\phi\left(|\widetilde{h}_{s,H_1}|^2\sigma_d^2 + \sigma_w^2\right)} \\ &\gtrless_{H_0}^{H_1} T_1, \end{aligned} \tag{27}$$

TABLE II
COMPARATIVE STUDY OF THE DETECTORS

Detectors	Channel Knowledge	Sensitivity to HWI	Performance
CH-GLRT	All	Only insensitive to ϕ in QAM	Overall the best
KS-GLRT	None	Only insensitive to ϕ in QAM	the worst among 4 detectors
KCI-GLRT	All	Only insensitive to ϕ in QAM	Only worse than CH-GLRT
KR-GLRT	h_s is unknown	Only insensitive to ϕ in QAM	Only better than KS-GLRT
Conventional detectors	the same as considering HWI	-	Always worse than considering HWI
RANGE-GLRT	None	Insensitive	Range limit: 33 km, range resolution : 30 m

where $D_s(\boldsymbol{s})$ are given in Appendix A. The derived detector Λ_1 is denoted as the KS-GLRT ('KS' means 'known s') detector. The derivation details are given in Appendix A.

C. GLRT with known h_r and h_s

In this case, we know the channel gains h_r and h_s while the transmitted signal $\boldsymbol{s}$ is unknown. Thus, $\hat{h}_{r,H_1} = \hat{h}_{r,H_0} = h_r$ and $\hat{h}_{s,H_1} = h_s$. Since each transmitted symbol s_i is independent, we can get the MLE of s_i for each sample separately. For H_0, we use (15) and (21) to have

$$\begin{aligned} f_0(s_i^R, s_i^I) = &\frac{a^2|h_r|^2\cos^2(\phi)B(\boldsymbol{s}) + a|h_r|\cos(\phi)C_r(\theta_r)}{a^2\cos^2\phi\left(|h_r|^2\sigma_d^2+\sigma_w^2\right)} \\ &+ \frac{a^2\sum_{i=1}^{I} {y_{r,i}^R}^2 - 2a\sin(\phi)\sum_{i=1}^{I} y_{r,i}^R y_{r,i}^I + \sum_{i=1}^{I} {y_{r,i}^I}^2}{a^2\cos^2\phi\left(|h_r|^2\sigma_d^2+\sigma_w^2\right)} \\ &+ I\ln\left(|h_r|^2\sigma_d^2+\sigma_w^2\right). \end{aligned} \tag{28}$$

For H_1 we use (14), (21) and (22) to have

$$\begin{aligned} f_1(s_i^R, s_i^I) = &I\ln\left(|h_s|^2\sigma_d^2+\sigma_w^2\right) \\ &+ \frac{\left(|h_s|^2\sigma_d^2+\sigma_w^2\right)\sum_{i=1}^{I} A_{ri} + \left(|h_r|^2\sigma_d^2+\sigma_w^2\right)\sum_{i=1}^{I} A_{si,H_1}}{a^2\cos^2\phi\left(|h_r|^2\sigma_d^2+\sigma_w^2\right)\left(|h_s|^2\sigma_d^2+\sigma_w^2\right)}. \end{aligned} \tag{29}$$

By letting the derivatives of (28) and (29) to be 0, one has the MLE of s_i under H_0 as $\hat{s}_{i,H_0}$ and the MLE of s_i under H_1 as $\hat{s}_{i,H_1}$. Substituting $\hat{s}_{i,H_0}$ and $\hat{s}_{i,H_1}$ into (14) and (15), one has

$$\begin{aligned} \Lambda_2 = &ln_{H_1} - ln_{H_0} \\ = &-I\ln\left(|h_s|^2\sigma_d^2+\sigma_w^2\right) + I\ln\sigma_w^2 + \frac{\sum_{i=1}^{I} A_{si,H_0}}{a^2\cos^2\phi\left(\sigma_w^2\right)} \\ &- \frac{|h_r|^2\sum_{i=1}^{I} A_{si,H_0} - 2|h_r||h_s|E(\theta)}{a^2\cos^2\phi\left(|h_r|^2\left(2\sigma_d^2|h_s|^2+\sigma_w^2\right)+|h_s|^2\sigma_w^2\right)} \\ &- \frac{|h_s|^2(a^2\sum_{i=1}^{I} {y_{r,i}^R}^2 - 2a\sin(\phi)\sum_{i=1}^{I} y_{r,i}^R y_{r,i}^I + \sum_{i=1}^{I} {y_{r,i}^I}^2)}{a^2\cos^2\phi\left(|h_r|^2\left(2\sigma_d^2|h_s|^2+\sigma_w^2\right)+|h_s|^2\sigma_w^2\right)} \\ &\gtrless_{H_0}^{H_1} T_2, \end{aligned} \tag{30}$$

where

$$E(\theta) = E_1\sin\theta + E_2\cos\theta, \tag{31}$$

$$E_1 = a\cos(\phi)\sum_{i=1}^{I} y_{r,i}^I y_{s,i}^R - a\cos(\phi)\sum_{i=1}^{I} y_{r,i}^R y_{s,i}^I, \tag{32}$$

and

$$\begin{aligned} E_2 = &a^2\left(\sum_{i=1}^{I} y_{r,i}^R y_{s,i}^R\right) - a\sin(\phi)\left(\sum_{i=1}^{I} y_{r,i}^R y_{s,i}^I\right) \\ &- a\sin(\phi)\left(\sum_{i=1}^{I} y_{r,i}^I y_{s,i}^R\right) + \sum_{i=1}^{I} y_{r,i}^I y_{s,i}^I. \end{aligned} \tag{33}$$

This detector Λ_2 is denoted as the KCI-GLRT ('KCI' means 'known channel information of h_s and h_r') detector. The derivation details are given in Appendix B.

D. GLRT with known h_r

In this case, we know the channel gain h_r while the transmitted signal $\boldsymbol{s}$ and h_s are unknown, so $\hat{h}_{r,H_1} = \hat{h}_{r,H_0} = h_r$. The reference channel could use reference symbols for channel estimation and therefore h_r is easier to obtain than h_s. Also, the MLE of s_i under H_0 as $\hat{s}_{i,H_0}$ and the MLE of s_i under H_1 as $\hat{s}_{i,H_1}$ are the same as those in KCI-GLRT.

Then, one can obtain the MLE of $|h_s|$ under H_1 as $|\widetilde{h}_{s,H_1}|$. Using $\hat{s}_{i,H_0}$, $\hat{s}_{i,H_1}$ and $|\widetilde{h}_{s,H_1}|$ in (14) and (15), the log-likelihood ratio finally becomes

$$\begin{aligned} \Lambda_3 = &ln_{H_1} - ln_{H_0} \\ = &-I\ln\left(|\widetilde{h}_{s,H_1}|^2\sigma_d^2+\sigma_w^2\right) + I\ln\sigma_w^2 + \frac{\sum_{i=1}^{I} A_{si,H_0}}{a^2\cos^2\phi\left(\sigma_w^2\right)} \\ &- \frac{|h_r|^2\sum_{i=1}^{I} A_{si,H_0} - 2|h_r||\widetilde{h}_{s,H_1}|\sqrt{E_1^2+E_2^2}}{a^2\cos^2\phi\left(|h_r|^2\left(2\sigma_d^2|\widetilde{h}_{s,H_1}|^2+\sigma_w^2\right)+|\widetilde{h}_{s,H_1}|^2\sigma_w^2\right)} \\ &- \frac{|\widetilde{h}_{s,H_1}|^2(a^2\sum_{i=1}^{I} {y_{r,i}^R}^2 - 2a\sin(\phi)\sum_{i=1}^{I} y_{r,i}^R y_{r,i}^I + \sum_{i=1}^{I} {y_{r,i}^I}^2)}{a^2\cos^2\phi\left(|h_r|^2\left(2\sigma_d^2|\widetilde{h}_{s,H_1}|^2+\sigma_w^2\right)+|\widetilde{h}_{s,H_1}|^2\sigma_w^2\right)} \\ &\gtrless_{H_0}^{H_1} T_3. \end{aligned} \tag{34}$$

The detector Λ_3 is denoted as the KR-GLRT ('KR' means 'known h_r') detector. The derivation details are given in Appendix C. To indicate the necessity of considering HWI, we also provide the corresponding conventional detectors ignoring the existence of IQI and AD for each novelly proposed detector as benchmarks in Appendix D.

IV. DETECTION WITH INTERFERING TARGET

In this section, the novel detector with an interfering target is also derived based on GRLT. For the RC, it receives a direct

arrival signal with a time delay of $\tau_r = L/c$, where L is the transmitter-receiver distance and c is the transmission velocity of radio. Thus, (3) becomes

$$x_{r,i} = h_r s_{l,i} + w_{r,i}, \tag{35}$$

with $s_{l,i} = s_{d,i-l_0}$ where $l_0 = \tau_r f_s$. Denote $\tau_s = R/c$, $\delta_s = \delta_R/c$, where R is the bistatic range of the desired target and δ_R is the difference of bistatic range between the interfering target and the desired target and $h_{s,2}$ is the SC channel gain of the interfering target. Under H_1 the SC signal contains the reflection of the desired signal, so

$$H_1 : x_{s,i} = h_{s,1} s_{l,i-l_1} + h_{s,2} s_{l,i-l_1-l_2} + w_{s,i}, \tag{36}$$

where $l_1 = \tau_s f_s$ and $l_2 = \delta_s f_s$. Under H_0 the SC signal consists of the reflection of one interfering target and the AWGN in the SC. Thus,

$$H_0 : x_{s,i} = h_{s,2} s_{l,i-l_1-l_2} + w_{s,i}, \tag{37}$$

where $h_{s,1}$ is the channel gain of the desired target in SC. Similarly, $x_{r,i}$ and $x_{s,i}$ suffer from HWI at the receiver to become (4).

Observing from (36) and (37), $x_{s,i}$ can be expressed by

$$H_0 : x_{s,i} = \beta x_{r,i-l_1-l_2} - \beta w_{r,i-l_1-l_2} + w_{s,i},$$

and

$$\begin{aligned} H_1 : x_{s,i} = {} & \alpha x_{r,i-l_1} + \beta x_{r,i-l_1-l_2} \\ & - \alpha w_{r,i-l_1} - \beta w_{r,i-l_1-l_2} + w_{s,i}, \end{aligned} \tag{38}$$

where $\alpha = h_{s,1}/h_r$ and $\beta = h_{s,2}/h_r$. According to [43], it is reasonable to assume that $\alpha \ll 1$ and $\beta \ll 1$ since the signal is severely attenuated in the SC compared with the RC. Therefore, one can approximate (38) as

$$H_0 : x_{s,i} = \beta x_{r,i-l_1-l_2} + w_{s,i},$$

and

$$H_1 : x_{s,i} = \alpha x_{r,i-l_1} + \beta x_{r,i-l_1-l_2} + w_{s,i}. \tag{39}$$

Thus, only the likelihood of $\mathbf{X_s} = (x_{s,1}, ..., x_{s,I})$ is required to make the detection. To explore the impact of L, R and δ_R, these parameters are predefined and known to the passive radar. MLE is used to estimate α and β. The likelihood of $\mathbf{X_s}$ is

$$\begin{cases} l_{H_1}(\mathbf{X_s}) = \frac{\exp\left(-\frac{1}{\sigma_w^2} l_1\right)}{(\pi\sigma_w^2)^I} \\ l_{H_0}(\mathbf{X_s}) = \frac{\exp\left(-\frac{1}{\sigma_w^2} l_0\right)}{(\pi\sigma_w^2)^I} \end{cases}, \tag{40}$$

where

$$l_1 = \sum_{i=1}^{I} \left| x_{s,i} - \alpha x_{r,i-l_1} - \beta x_{r,i-l_1-l_2} \right|^2,$$

and

$$l_0 = \sum_{i=1}^{I} \left| x_{s,i} - \beta x_{r,i-l_1-l_2} \right|^2.$$

By (39) and (40), we mitigate the effect of HWI. σ_w is firstly assumed to be fixed and known, then one obtains that

$$\begin{bmatrix} \hat{\beta}_1 \\ \hat{\alpha} \end{bmatrix} = \begin{bmatrix} r_{ii}^{-1} + g r_{ii}^{-2} |r_{si}|^2 & -g r_{ii}^{-1} r_{si} \\ -g r_{si}^* r_{ii}^{-1} & g \end{bmatrix} \begin{bmatrix} r_{xi} \\ r_{xs} \end{bmatrix}, \tag{41}$$

TABLE III
SIMULATION PARAMETER SETUP

Parameter	Value
P for non RANGE-GLRT	1
P for RANGE-GLRT	100
IO for non RANGE-GLRT	64-QAM or 64-PSK
IO for RANGE-GLRT	DVB-T
f_s	9.14 MHz
σ_w^2	1
σ^2	1
SNR_r	10 dB
$\mathrm{SNR}_{s,1}$	-7 dB
$\mathrm{SNR}_{s,2}$	-7 dB
T_0	3
T_1	15
T_2	30
T_3	35
T_4	5
Monte Carlo runs	10000

where

$$\begin{cases} r_{ii} = \sum_{i=1}^{I} |x_{r,i-l_1-l_2}|^2 \\ r_{ss} = \sum_{i=1}^{I} |x_{r,i-l_1}|^2 \\ r_{xi} = \sum_{i=1}^{I} x_{s,i} x_{r,i-l_1-l_2}^* \\ r_{xs} = \sum_{i=1}^{I} x_{s,i} x_{r,i-l_1}^* \\ r_{si} = \sum_{i=1} x_{r,i-l_1} x_{r,i-l_1-l_2}^* \end{cases}, \tag{42}$$

and

$$g = (r_{ss} - r_{ii}^{-1} |r_{si}|^2)^{-1}. \tag{43}$$

(41) is the MLEs of α and β under H_1. Similarly, one has the MLE of β under H_0 as

$$\hat{\beta}_0 = r_{ii}^{-1} r_{xi}. \tag{44}$$

Therefore, the MLE of σ_w^2 under H_1 is

$$\hat{\sigma}_{w,1}^2 = \frac{l_1}{I}, \tag{45}$$

and the MLE of σ_w^2 under H_0 is

$$\hat{\sigma}_{w,0}^2 = \frac{l_0}{I}. \tag{46}$$

Using (45) and (46), the GLRT is expressed as

$$\frac{l_{H_1}(\mathbf{X_s})}{l_{H_0}(\mathbf{X_s})} = \left(\frac{\sum_{i=1}^{I} |x_s[i]|^2 - r_{ii} |\hat{\beta}_0|^2}{\sum_{i=1}^{I} |x_s[i]|^2 - r_{ii} |\hat{\beta}_0|^2 - g^{-1} |\hat{\alpha}|^2}\right)^I \geq \eta. \tag{47}$$

From (47), one has

$$\Lambda_4 = \frac{g^{-1} |\hat{\alpha}|^2}{\sum_{i=1}^{I} |x_s[i]|^2 - r_{ii} |\hat{\beta}_0|^2} \geq T_4. \tag{48}$$

Denote $\mathbf{X}_i = (x_{r,1-l_1-l_2}, ..., x_{r,I-l_1-l_2})^T$ and $\mathbf{X}_0 = (x_{r,1-l_1}, ..., x_{r,I-l_1})^T$. The projection matrix that projects a vector onto $\mathbf{X}_i$ is $\mathbf{M} = (\mathbf{X}_i^H \mathbf{X}_i)^{-1} \mathbf{X}_i \mathbf{X}_i^H$, so $\mathbf{M}^\perp = \mathbf{I} - \mathbf{M}$ is the orthogonal projection matrix that projects a vector onto the space orthogonal to that spanned by $\mathbf{X}_i$. Using the definitions of $\mathbf{X}_i$, $\mathbf{X}_0$, $\mathbf{M}$ and $\mathbf{M}^\perp$, one has $r_{si} = \mathbf{X}_i^H \mathbf{X}_0$, $r_{xi} = \mathbf{X}_i^H \mathbf{X}_s$, $r_{xs} = \mathbf{X}_0^H \mathbf{X}_s$, $r_{ss} = \mathbf{X}_0^H \mathbf{X}_0$ and $r_{ii} = \mathbf{X}_i^H \mathbf{X}_i$. Therefore, according to [43], the detector Λ_4 becomes

$$\Lambda_4 = \frac{|\mathbf{X}_0^H \mathbf{M}^\perp \mathbf{X}_s|^2}{(\mathbf{X}_0^H \mathbf{M}^\perp \mathbf{X}_0)(\mathbf{X}_s^H \mathbf{M}^\perp \mathbf{X}_s)} \geq T_4. \tag{49}$$

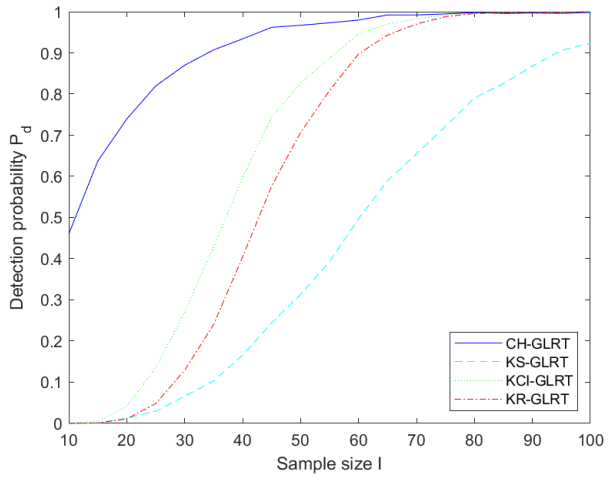

Fig. 1. Detection probability P_d of the proposed detectors versus sample size I with SNR_r = 0 dB , SNR_s = -7 dB , $\sigma^2 = 1.0$, $a = 0.9$ and $\phi = 10°$.

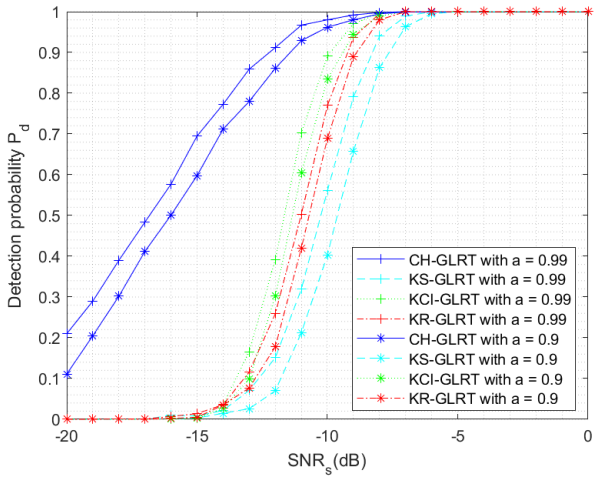

Fig. 2. P_d of the proposed detectors versus SNR_s under different a with SNR_r = 0 dB , $\sigma^2 = 1.0$, $\phi = 0°$ and $I = 100$.

(49) can be regarded as the square of correlation parameter between the projection of the received vector $\mathbf{X}_s$ onto the signal subspace and the desired target delayed vector $\mathbf{X}_0$ onto the signal subspace. This statistic Λ_4 is denoted as RANGE-GLRT detector.

V. Numerical Results and Discussion

In this section, the new detectors are compared with the conventional detectors as benchmarks in the detection probability P_d. The transmitted signal s from IO is generated using 64-quadrature amplitude modulation (QAM) scheme unless specified otherwise. The comparison is performed using Monte Carlo simulation to demonstrate the superiority of the proposed detectors over the conventional ones. Each curve is averaged over 10000 runs. The SNR in RC is denoted as $\mathrm{SNR_r} = 10\log_{10}\frac{|h_r|^2}{\sigma_w^2}$ and the SNR in SC is denoted as $\mathrm{SNR_s} = 10\log_{10}\frac{|h_s|^2}{\sigma_w^2}$. The threshold for each proposed detector is determined by fixing the false alarm probability to 0.01, which gives a threshold of 3, 15, 30 and 35 for CH-GLRT, KS-GLRT, KCI-GLRT and KR-GLRT, respectively. We fix $\sigma_w^2 = 1$, $\mathrm{SNR_r} = 10$ dB , $\sigma^2 = \sigma_t^2 + \sigma_r^2 = 1$ and $P = 1$ while changing $\mathrm{SNR_s}$, a, ϕ and I.

The sample size I is studied first. We set $\mathrm{SNR_r} = 10$ dB , $\mathrm{SNR_s} = -7$ dB , $a = 0.9$, $\phi = 10°$ and $\sigma^2 = 1.0$. All four proposed detectors are compared in terms of the detection performance. It is illustrated in Fig. 1 that all detectors improve as I increases because more samples give more accurate detection. As expected, CH-GLRT detector is the best since it knows all the necessary parameters in the detection. KCI-GLRT outperforms KR-GLRT by having extra information of h_s. KS-GLRT is the worst when only the transmitted signal s is known. Thus, knowing s is less valuable than knowing the channel gains in passive radar detection. Next, we let $\sigma^2 = 1$ and $\phi = 0°$ while a is varying. Other parameters are set as SNR_r = 10 dB , $\sigma^2 = 1.0$, $\phi = 0°$ and $I = 100$ to examine the impact of amplitude mismatch a on the detection performance in Fig. 2. One can observe that a has a significant impact on the overall performance. A smaller a represents a more

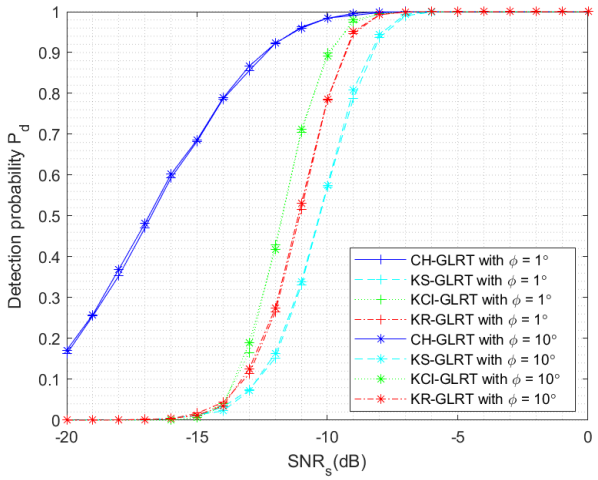

Fig. 3. P_d of the proposed detectors versus SNR_s under different ϕ for 64-QAM with SNR_r = 0 dB , $\sigma^2 = 1.0$, $a = 1$ and $I = 100$.

severe amplitude mismatch. The effect of phase mismatch ϕ is examined in Fig. 3 and Fig. 4. In this case, we vary ϕ from 1° to 10° with $a = 1.0$ while other parameters are the same as those in Fig. 2. The result in Fig. 3 shows that ϕ has little impact on the detection performance when the transmitted signal uses 64-QAM modulation. Considering that the QAM method employs both amplitude and phase to differentiate the information symbols, a pure phase mismatch might not affect the detection of the target much. To verify this, Fig. 4 provides the performance comparison for phase-shift keying (PSK), where all parameters are the same as those in Fig. 3. In Fig. 4, ϕ has a considerable impact on the detection performance since the phase mismatch of 10° exceeds the approximate phase interval of 5.62° for two neighboring information symbols in 64-PSK modulation and severely distorts the signal. In this regard, QAM is more robust to phase mismatch than PSK. We also note that the phase mismatch ϕ has less impact on the detection performance than the amplitude mismatch a, as a causes larger performance degradation by comparing Fig. 2 and Fig. 4.

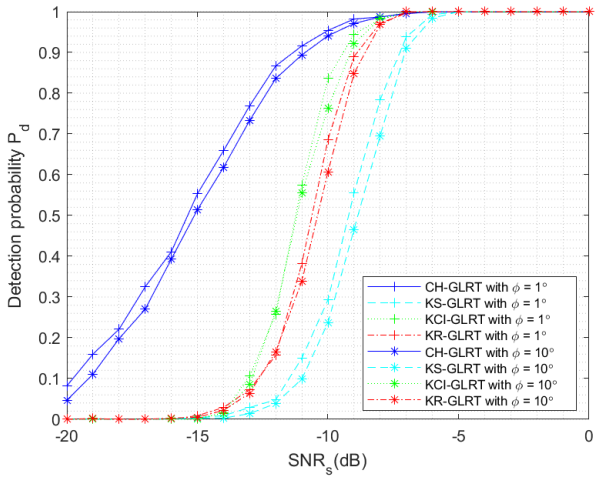

Fig. 4. P_d of the proposed detectors versus SNR_s under different ϕ for 64-PSK with SNR_r = 0 dB , $\sigma^2 = 1.0$, $a = 1$ and $I = 100$.

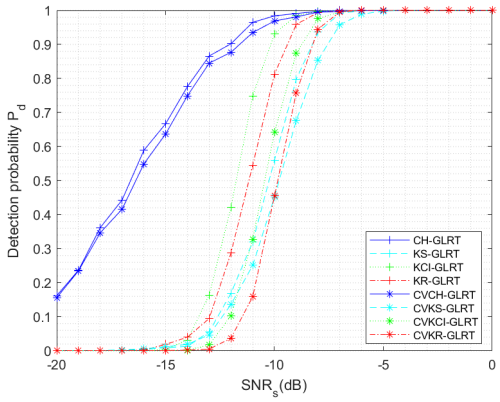

Fig. 5. Comparison of P_d between proposed detectors and the conventional detectors with $\sigma^2 = 1.0$, $a = 0.99$, $\phi = 1^\circ$ and $I = 100$.

Next, we compare the performances of the proposed detectors considering HWI and the corresponding conventional detectors ignoring HWI. The case with negligible IQI is represented by $a = 0.99$ and $\phi = 1^\circ$. With a sample size $I = 100$, $\sigma^2 = 1.0$ and $\mathrm{SNR}_r = 10$ dB , we show the comparison in Fig. 5. It can be seen that the proposed detectors outperform their corresponding conventional ones, which indicates that the detector is very sensitive to the non-ideality of the transceiver and that this sensitivity is different for different detectors. Therefore, it is pretty necessary to derive the new detectors for HWI.

Different from the four new detectors presented previously, RANGE-GLRT uses the DVB-T signals. It must consider the time delay and the path loss due to the long bistatic range and interfering target. Therefore, P and I are set to be 100 and 1000, respectively. $\mathrm{SNR}_{s,1}$ and $\mathrm{SNR}_{s,2}$ are fixed to be -7 dB to study the effects of L, R and δ_R. It is illustrated in Fig. 6 that a range limit of about 33 km exists for the RANGE-GLRT detector. Such a range limit is the sum of the bistatic range and the transmitter-receiver distance, which is also the sum of the distance from the target to the transmitter and the distance from the target to the receiver. The passive radar can no longer detect the desired target when the range is beyond the limit.

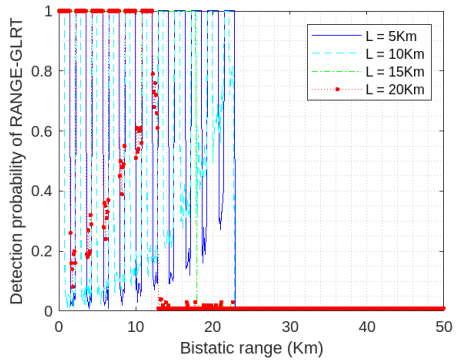

Fig. 6. The effect of bistatic range R with $\delta_R = 1$ km, $\sigma^2 = 1.0$, $a = 0.9$, $\phi = 5^\circ$, $\mathrm{SNR}_r = 10$ dB , $\mathrm{SNR}_{s,1} = -7$ dB , $\mathrm{SNR}_{s,2} = -7$ dB and $I = 1000$.

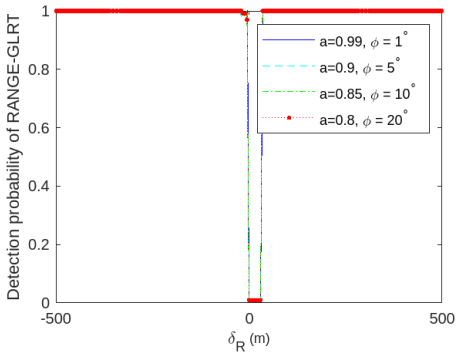

Fig. 7. The effect of δ_R with $\sigma^2 = 1.0$, L = 10 km, R = 15 km, $\mathrm{SNR}_r = 10$ dB , $\mathrm{SNR}_{s,1} = -7$ dB , $\mathrm{SNR}_{s,2} = -7$ dB and $I = 1000$.

When L is fixed, increasing R within its range limit is always feasible for better detection performance. Interestingly, some periodic range intervals perform poorly in detecting the desired target, indicating that the detection probability is not linearly correlated with R. Only the green dotted line of $L = 15$ km keeps the ideal detection probability of 1 before R reaches its maximum of 18 km. Thus, these different performance patterns make the green line 'invisible' as it overlaps with the other three lines. This phenomenon is consistent with [44]. Finally, we investigate the range resolution of RANGE-GLRT in Fig. 7. Fix $L = 10$ km and $R = 15$ km, the range resolution is measured by the interval of δ_R where the desired target is 'covered' or 'dissembled' by the interfering target so that the passive radar cannot detect it. The range resolution is about 30 m which is very close to the theoretical one of DVB-T [20]. Also, the range resolution is not affected by the level of HWI, which proves that our proposed HWI mitigation algorithm is effective.

VI. Conclusions

Several novel passive radar detectors have been proposed based on different channel and signal information knowledge considering both IQI and AD. For the single-target passive radar, numerical results have demonstrated that HWI does have a significant impact on the overall detection performance and that the destructive effects of IQI should not be ignored even when the amplitude mismatch and the phase mismatch are

small. The amplitude mismatch has a much more degrading impact than the phase mismatch in general. Furthermore, the HWI mitigation algorithm has been proposed to develop the RANGE-GLRT detector to investigate the effect of range and range resolution. This detector is demonstrated to have robust range resolution regardless of the IQI level. Finally, the sample size can improve the overall detection performance.

APPENDIX

A. Derivation of KS-GLRT Detector

According to (26), by solving the equation $\frac{\partial f_0(|h_r|,\theta_r)}{\partial \theta_r}=0$, we obtain the MLE of θ_r under H_0 as

$$\hat{\theta}_{r,H_0}=-\frac{\pi}{2}-\arctan\frac{D_{r2}(\boldsymbol{s})}{D_{r1}(\boldsymbol{s})}, \tag{50}$$

where

$$\begin{aligned}D_{r1}(\boldsymbol{s})&=\left(-a^2\sin^2(\phi)+a^2\cos^2(\phi)+a^2\right)\sum_{i=1}^{I}s_i^I y_{r,i}^R\\&+\left(2a\sin(\phi)-2a^2\sin(\phi)\cos(\phi)\right)\sum_{i=1}^{I}s_i^R y_{r,i}^R-2\sum_{i=1}^{I}s_i^R y_{r,i}^I,\end{aligned} \tag{51}$$

and

$$\begin{aligned}D_{r2}(\boldsymbol{s})&=2a\sin(\phi)\left(\sum_{i=1}^{I}s_i^R y_{r,i}^I\right)-2a\cos(\phi)\left(\sum_{i=1}^{I}s_i^I y_{r,i}^I\right)\\&+\left(-a^2\sin^2(\phi)+a^2\cos^2(\phi)-a^2-2a\cos(\phi)\right)\sum_{i=1}^{I}s_i^R y_{r,i}^R\\&+2a^2\sin(\phi)\cos(\phi)\left(\sum_{i=1}^{I}s_i^I y_{r,i}^R\right).\end{aligned} \tag{52}$$

$D_{r1}(\boldsymbol{s})$ and $D_{r2}(\boldsymbol{s})$ are known constants which only depend on $\boldsymbol{s}$. However, $\frac{\partial f_0(|h_r|,\theta_r)}{\partial |h_r|}=0$ does not lead to an analytical solution since $\frac{\partial f_0(|h_r|,\theta_r)}{\partial |h_r|}$ is a cubic function of $|h_r|$. This equation can be solved by using MATLAB functions. Denote its numerical solution as $|\widetilde{h}_{r,H_0}|$. One has

$$|\hat{h}_{r,H_0}|=|\widetilde{h}_{r,H_0}|, \tag{53}$$

and

$$\hat{h}_{r,H_0}=|\widetilde{h}_{r,H_0}|e^{j\hat{\theta}_{r,H_0}}, \tag{54}$$

where $\hat{\theta}_{r,H_0}$ is given in (50). The MLE of h_r under H_0 and H_1 is the same, i.e. $\hat{h}_{r,H_1}=\hat{h}_{r,H_0}$. Similarly, we can obtain $\hat{h}_{s,H_1}$ as

$$\begin{cases}\hat{\theta}_{s,H_1}=-\frac{\pi}{2}-\arctan\frac{D_{s2}(\boldsymbol{s})}{D_{s1}(\boldsymbol{s})}\\ |\hat{h}_{s,H_1}|=|\widetilde{h}_{s,H_1}|\\ \hat{h}_{s,H_1}=|\widetilde{h}_{s,H_1}|e^{j\hat{\theta}_{s,H_1}}\end{cases}, \tag{55}$$

where

$$\begin{aligned}D_{s1}(\boldsymbol{s})&=\left(-a^2\sin^2(\phi)+a^2\cos^2(\phi)+a^2\right)\sum_{i=1}^{I}s_i^I y_{s,i}^R\\&+\left(2a\sin(\phi)-2a^2\sin(\phi)\cos(\phi)\right)\sum_{i=1}^{I}s_i^R y_{s,i}^R-2\sum_{i=1}^{I}s_i^R y_{s,i}^I,\end{aligned} \tag{56}$$

and

$$\begin{aligned}D_{s2}(\boldsymbol{s})&=2a\sin(\phi)\left(\sum_{i=1}^{I}s_i^R y_{s,i}^I\right)-2a\cos(\phi)\left(\sum_{i=1}^{I}s_i^I y_{s,i}^I\right)\\&+\left(-a^2\sin^2(\phi)+a^2\cos^2(\phi)-a^2-2a\cos(\phi)\right)\sum_{i=1}^{I}s_i^R y_{s,i}^R\\&+2a^2\sin(\phi)\cos(\phi)\left(\sum_{i=1}^{I}s_i^I y_{s,i}^R\right).\end{aligned} \tag{57}$$

Denote $D_r(\boldsymbol{s})=\sqrt{D_{r1}(\boldsymbol{s})^2+D_{r2}(\boldsymbol{s})^2}$ and $D_s(\boldsymbol{s})=\sqrt{D_{s1}(\boldsymbol{s})^2+D_{s2}(\boldsymbol{s})^2}$. Therefore, by substituting (54) and (55) into (14) and (15), one has (27).

B. Derivation of KCI-GLRT Detector

According to (28), by solving the simultaneous equations

$$\begin{cases}\frac{\partial f_0(s_i^R,s_i^I)}{\partial s_i^R}=0\\ \frac{\partial f_0(s_i^R,s_i^I)}{\partial s_i^I}=0\end{cases}, \tag{58}$$

we obtain $\hat{s}_{i,H_0}$ as

$$\hat{s}_{i,H_0}^R=\frac{a y_{r,i}^R\cos(\theta_r+\phi)+\sin(\theta_r)\,y_{s,i}^I}{a\cos(\phi)|h_r|}, \tag{59}$$

$$\begin{aligned}\hat{s}_{i,H_0}^I&=\frac{a y_{r,i}^R\left(a\sin(\theta_r+2\phi)-a\sin(\theta_r)-2\sin(\theta_r+\phi)\right)}{2a^2\cos^2(\phi)|h_r|}\\&+\frac{2y_{r,i}^I\left(a\sin(\phi)\sin(\theta_r)+\cos(\theta_r)\right)}{2a^2\cos^2(\phi)|h_r|},\end{aligned} \tag{60}$$

and

$$\hat{s}_{i,H_0}=\hat{s}_{i,H_0}^R+i\hat{s}_{i,H_0}^I. \tag{61}$$

Similarly, by solving the simultaneous equations

$$\begin{cases}\frac{\partial f_1(s_i^R,s_i^I)}{\partial s_i^R}=0\\ \frac{\partial f_1(s_i^R,s_i^I)}{\partial s_i^I}=0\end{cases}, \tag{62}$$

one has $\hat{s}_{i,H_1}=\hat{s}_{i,H_1}^R+i\hat{s}_{i,H_1}^I$. Therefore, by substituting $\hat{s}_{i,H_0}$ and $\hat{s}_{i,H_1}$ into (14) and (15), one has (30).

C. Derivation of KR-GLRT Detector

To obtain $\hat{s}_{i,H_1}$, we have from (14), (21) and (22)

$$\begin{aligned}f_1(s_i^R,s_i^I,\theta_s,|h_s|)&=I\ln\left(|h_s|^2\sigma_d^2+\sigma_w^2\right)\\&+\frac{\left(|h_s|^2\sigma_d^2+\sigma_w^2\right)\sum_{i=1}^{I}A_{ri}+\left(|h_r|^2\sigma_d^2+\sigma_w^2\right)\sum_{i=1}^{I}A_{si,H_1}}{a^2\cos^2\phi\left(|h_r|^2\sigma_d^2+\sigma_w^2\right)\left(|h_s|^2\sigma_d^2+\sigma_w^2\right)},\end{aligned} \tag{63}$$

which is the same as (29), so $\hat{s}_{i,H_1}$ is also obtained by solving (62). Substitute $\hat{s}_{i,H_1}$ into (63), it becomes

$$\begin{aligned}f_2(|h_s|,\theta_s)&=\frac{|h_r|^2\sum_{i=1}^{I}A_{si,H_0}-2|h_r||h_s|F(\theta_s)}{a^2\cos^2\phi\left(|h_r|^2\left(2\sigma_d^2|h_s|^2+\sigma_w^2\right)+|h_s|^2\sigma_w^2\right)}\\&+\frac{|h_s|^2\left(a^2\sum_{i=1}^{I}{y_{r,i}^R}^2-2a\sin(\phi)\sum_{i=1}^{I}y_{r,i}^R y_{r,i}^I+\sum_{i=1}^{I}{y_{r,i}^I}^2\right)}{a^2\cos^2\phi\left(|h_r|^2\left(2\sigma_d^2|h_s|^2+\sigma_w^2\right)+|h_s|^2\sigma_w^2\right)}\\&+I\ln\left(|h_s|^2\sigma_d^2+\sigma_w^2\right),\end{aligned} \tag{64}$$

where

$$F(\theta_s) = F_1(\theta_r)\sin\theta_s + F_2(\theta_r)\cos\theta_s, \tag{65}$$

$$F_1(\theta_r) = E_2\sin\theta_r - E_1\cos\theta_r, \tag{66}$$

and

$$F_2(\theta_r) = E_1\sin\theta_r + E_2\cos\theta_r. \tag{67}$$

Therefore, by solving the equation $\frac{\partial f_2(|h_s|,\theta_s)}{\partial\theta_s} = 0$, one obtains

$$\hat{\theta}_{s,H_1} = \frac{\pi}{2} - \arctan\frac{F_2(\theta_r)}{F_1(\theta_r)}. \tag{68}$$

Again, $\frac{\partial f_2(|h_s|,\theta_s)}{\partial|h_s|} = 0$ does not have a closed-form solution and its numerical solution using MATLAB is denoted as $|\widetilde{h}_{s,H_1}|$ to give

$$|\hat{h}_{s,H_1}| = |\widetilde{h}_{s,H_1}|, \tag{69}$$

and

$$\hat{h}_{s,H_1} = |\widetilde{h}_{s,H_1}|e^{j\hat{\theta}_{s,H_1}}. \tag{70}$$

Then, $\hat{s}^R_{i,H_1}$ and $\hat{s}^I_{i,H_1}$ are also obtained and $\hat{s}_{i,H_1} = \hat{s}^R_{i,H_1} + i\hat{s}^I_{i,H_1}$. Using $\hat{h}_{s,H_1}$ and $\hat{s}_{i,H_1}$ in (14) and (15), one obtains (34).

D. Conventional Detectors ignoring HWI

Here, we derive the corresponding conventional detectors ignoring the existence of IQI and AD. These detectors are used as benchmarks for comparison. The system model in (3) ignoring HWI becomes

$$H_0: \begin{cases} y_{r,i} = h_r s_i + w_{r,i} \\ y_{s,i} = w_{s,i} \end{cases}, H_1: \begin{cases} y_{r,i} = h_r s_i + w_{r,i} \\ y_{s,i} = h_s s_i + w_{s,i}. \end{cases} \tag{71}$$

When all parameters are known, it can be shown that the conventional coherent detector ignoring HWI is

$$\Lambda_{c0} = -\frac{\sum_{i=1}^{I}|y_{s,i} - h_s s_i|^2}{\sigma_w^2} + \frac{\sum_{i=1}^{I}|y_{s,i}|^2}{\sigma_w^2} \gtrless_{H_0}^{H_1} T_{c0}, \tag{72}$$

which is denoted as the CVCH-GLRT ('CVCH' means the 'conventional coherent') detector.

When only $\boldsymbol{s}$ is known, the conventional detector from [26] is

$$\Lambda_{c1} = -\frac{\sum_{i=1}^{I}|y_{s,i} - \frac{\boldsymbol{s}^{\mathrm{T}}\boldsymbol{y_s}}{\boldsymbol{s}^{\mathrm{T}}\boldsymbol{s}}s_i|^2}{\sigma_w^2} + \frac{\sum_{i=1}^{I}|y_{s,i}|^2}{\sigma_w^2} \gtrless_{H_0}^{H_1} T_{c1}, \tag{73}$$

which is denoted as the CVKS-GLRT ('CVKS' means the 'conventional known $\mathbf{s}$') detector.

When both h_r and h_s are known, one can show that

$$\begin{aligned}\Lambda_{c2} &= \frac{2|h_r||h_s|\sin(\theta)\left(\sum_i^n y^I_{r,i}y^R_{s,i} - \sum_i^n y^R_{r,i}y^I_{s,i}\right)}{\sigma_w^2(|h_r|^2+|h_s|^2)} \\ &+ \frac{2|h_r||h_s|\cos(\theta)\left(\sum_i^n y^R_{r,i}y^R_{s,i} + \sum_i^n y^I_{r,i}y^I_{s,i}\right)}{\sigma_w^2(|h_r|^2+|h_s|^2)} \\ &- \frac{|h_r|^2\left({y^R_{s,i}}^2 + {y^I_{s,i}}^2\right) + |h_s|^2\left({y^R_{r,i}}^2 + {y^I_{r,i}}^2\right)}{\sigma_w^2(|h_r|^2+|h_s|^2)} + \frac{\sum_{i=1}^{I}|y_{s,i}|^2}{\sigma_w^2} \\ &\gtrless_{H_0}^{H_1} T_2,\end{aligned} \tag{74}$$

which is denoted as the CVKCI-GLRT ('CVKCI' means the 'conventional known channel information of h_r and h_s') detector.

When only h_r is known, the conventional detector ignoring HWI can be shown as

$$\begin{aligned}\Lambda_{c3} &= -\frac{|h_r|^2\left({y^R_{s,i}}^2 + {y^I_{s,i}}^2\right) + |\widetilde{h}_{s,H_1}|^2\left({y^R_{r,i}}^2 + {y^I_{r,i}}^2\right)}{\sigma_w^2(|h_r|^2+|\widetilde{h}_{s,H_1}|^2)} \\ &+ \frac{2|h_r||\widetilde{h}_{s,H_1}|F(\boldsymbol{y}_r,\boldsymbol{y}_s)}{\sigma_w^2(|h_r|^2+|\widetilde{h}_{s,H_1}|^2)} + \frac{\sum_{i=1}^{I}|y_{s,i}|^2}{\sigma_w^2} \\ &\gtrless_{H_0}^{H_1} T_3,\end{aligned} \tag{75}$$

where $|\widetilde{h}_{s,H_1}|$ is the approximate MLE of $|h_{s,H_1}|$ and

$$F(\boldsymbol{y}_r,\boldsymbol{y}_s) = \sqrt{\left(\sum_i^n y^I_{r,i}y^R_{s,i} - \sum_i^n y^R_{r,i}y^I_{s,i}\right)^2 + \left(\sum_i^n y^R_{r,i}y^R_{s,i} + \sum_i^n y^I_{r,i}y^I_{s,i}\right)^2}. \tag{76}$$

This is denoted as the CVKR-GLRT ('CVKR' means the 'conventional known h_r') detector.

REFERENCES

[1] F. Hu, B. Chen, and K. Zhu, "Full spectrum sharing in cognitive radio networks toward 5g: A survey," *IEEE Access*, vol. 6, pp. 15 754–15 776, 2018.

[2] N. J. Myers and R. W. Heath, "Infocus: A spatial coding technique to mitigate misfocus in near-field los beamforming," *IEEE Transactions on Wireless Communications*, vol. 21, no. 4, pp. 2193–2209, 2021.

[3] H. Zhang, N. Shlezinger, F. Guidi, D. Dardari, M. F. Imani, and Y. C. Eldar, "Beam focusing for near-field multiuser mimo communications," *IEEE Transactions on Wireless Communications*, vol. 21, no. 9, pp. 7476–7490, 2022.

[4] R. Bajracharya, R. Shrestha, Y. B. Zikria, and S. W. Kim, "Lte in the unlicensed spectrum: A survey," *IETE Technical Review*, vol. 35, no. 1, pp. 78–90, 2018.

[5] A. M. Cavalcante, E. Almeida, R. D. Vieira, S. Choudhury, E. Tuomaala, K. Doppler, F. Chaves, R. C. Paiva, and F. Abinader, "Performance evaluation of lte and wi-fi coexistence in unlicensed bands," in *2013 IEEE 77th Vehicular Technology Conference (VTC Spring)*. IEEE, 2013, pp. 1–6.

[6] H. He, H. Shan, A. Huang, Q. Ye, and W. Zhuang, "Edge-aided computing and transmission scheduling for lte-u-enabled iot," *IEEE Transactions on Wireless Communications*, vol. 19, no. 12, pp. 7881–7896, 2020.

[7] M. Song, C. Xin, Y. Zhao, and X. Cheng, "Dynamic spectrum access: from cognitive radio to network radio," *IEEE Wireless Communications*, vol. 19, no. 1, pp. 23–29, 2012.

[8] J. A. Ansere, G. Han, H. Wang, C. Choi, and C. Wu, "A reliable energy efficient dynamic spectrum sensing for cognitive radio iot networks," *IEEE Internet of Things Journal*, vol. 6, no. 4, pp. 6748–6759, 2019.

[9] J. Yang, S. Xiao, B. Jiang, H. Song, S. Khan, and S. Ul Islam, "Cache-enabled unmanned aerial vehicles for cooperative cognitive radio networks," *IEEE wireless communications*, vol. 27, no. 2, pp. 155–161, 2020.

[10] F. Miramirkhani and M. Uysal, "Channel modeling and characterization for visible light communications," *IEEE Photonics Journal*, vol. 7, no. 6, pp. 1–16, 2015.

[11] A. Al-Kinani, C.-X. Wang, H. Haas, and Y. Yang, "Characterization and modeling of visible light communication channels," in *2016 IEEE 83rd Vehicular Technology Conference (VTC Spring)*. IEEE, 2016, pp. 1–5.

[12] A. R. Chiriyath, B. Paul, and D. W. Bliss, "Radar-communications convergence: Coexistence, cooperation, and co-design," *IEEE Transactions on Cognitive Communications and Networking*, vol. 3, no. 1, pp. 1–12, 2017.

[13] Z. Feng, Z. Fang, Z. Wei, X. Chen, Z. Quan, and D. Ji, "Joint radar and communication: A survey," *China Communications*, vol. 17, no. 1, pp. 1–27, 2020.
[14] F. Liu, C. Masouros, A. Li, H. Sun, and L. Hanzo, "Mu-mimo communications with mimo radar: From co-existence to joint transmission," *IEEE Transactions on Wireless Communications*, vol. 17, no. 4, pp. 2755–2770, 2018.
[15] X. Liu, T. Huang, N. Shlezinger, Y. Liu, J. Zhou, and Y. C. Eldar, "Joint transmit beamforming for multiuser mimo communications and mimo radar," *IEEE Transactions on Signal Processing*, vol. 68, pp. 3929–3944, 2020.
[16] L. Zheng, M. Lops, and X. Wang, "Adaptive interference removal for uncoordinated radar/communication coexistence," *IEEE Journal of Selected Topics in Signal Processing*, vol. 12, no. 1, pp. 45–60, 2017.
[17] N. Nartasilpa, A. Salim, D. Tuninetti, and N. Devroye, "Communications system performance and design in the presence of radar interference," *IEEE Transactions on Communications*, vol. 66, no. 9, pp. 4170–4185, 2018.
[18] B. Li, A. P. Petropulu, and W. Trappe, "Optimum co-design for spectrum sharing between matrix completion based mimo radars and a mimo communication system," *IEEE Transactions on Signal Processing*, vol. 64, no. 17, pp. 4562–4575, 2016.
[19] Q. He, Z. Wang, J. Hu, and R. S. Blum, "Performance gains from cooperative mimo radar and mimo communication systems," *IEEE Signal Processing Letters*, vol. 26, no. 1, pp. 194–198, 2018.
[20] H. Kuschel, D. Cristallini, and K. E. Olsen, "Tutorial: Passive radar tutorial," *IEEE Aerospace and Electronic Systems Magazine*, vol. 34, no. 2, pp. 2–19, 2019.
[21] D. K. Tan, H. Sun, Y. Lu, M. Lesturgie, and H. L. Chan, "Passive radar using global system for mobile communication signal: theory, implementation and measurements," *IEE Proceedings-Radar, Sonar and Navigation*, vol. 152, no. 3, pp. 116–123, Jun. 2005.
[22] X.-l. Chen and H. Zhang, "Detection performance of passive bistatic radar based on ncaf," in *2019 IEEE International Conference on Signal, Information and Data Processing (ICSIDP)*. IEEE, 2019, pp. 1–5.
[23] X. Zhang, H. Li, and B. Himed, "A direct-path interference resistant passive detector," *IEEE Signal Processing Letters*, vol. 24, no. 6, pp. 818–822, Jun. 2017.
[24] F. Colone, C. Palmarini, T. Martelli, and E. Tilli, "Sliding extensive cancellation algorithm for disturbance removal in passive radar," *IEEE Transactions on Aerospace and Electronic Systems*, vol. 52, no. 3, pp. 1309–1326, 2016.
[25] C. Berthillot, A. Santori, O. Rabaste, D. Poullin, and M. Lesturgie, "Bem reference signal estimation for an airborne passive radar antenna array," *IEEE Transactions on Aerospace and Electronic Systems*, vol. 53, no. 6, pp. 2833–2845, 2017.
[26] G. Cui, J. Liu, H. Li, and B. Himed, "Signal detection with noisy reference for passive sensing," *Signal Processing*, vol. 108, pp. 389–399, 2015.
[27] J. Liu, H. Li, and B. Himed, "On the performance of the cross-correlation detector for passive radar applications," *Signal Processing*, vol. 113, pp. 32–37, 2015.
[28] J. L. Garry, C. J. Baker, and G. E. Smith, "Evaluation of direct signal suppression for passive radar," *IEEE Transactions on Geoscience and Remote Sensing*, vol. 55, no. 7, pp. 3786–3799, Jul. 2017.
[29] G. Fang, J. Yi, X. Wan, Y. Liu, and H. Ke, "Experimental research of multistatic passive radar with a single antenna for drone detection," *IEEE Access*, vol. 6, pp. 33 542–33 551, 2018.
[30] S. Javed, O. Amin, S. S. Ikki, and M.-S. Alouini, "Asymmetric modulation for hardware impaired systems—error probability analysis and receiver design," *IEEE Transactions on Wireless Communications*, vol. 18, no. 3, pp. 1723–1738, Mar. 2019.
[31] J. Li, M. Matthaiou, and T. Svensson, "I/q imbalance in af dual-hop relaying: Performance analysis in nakagami-m fading," *IEEE transactions on communications*, vol. 62, no. 3, pp. 836–847, Mar. 2014.
[32] T. C. Schenk, E. R. Fledderus, and P. F. Smulders, "Performance analysis of zero-if mimo ofdm transceivers with iq imbalance." *J. Commun.*, vol. 2, no. 7, pp. 9–19, 2007.
[33] X. Li, M. Liu, C. Deng, P. T. Mathiopoulos, Z. Ding, and Y. Liu, "Full-duplex cooperative noma relaying systems with i/q imbalance and imperfect sic," *IEEE Wireless Communications Letters*, vol. 9, no. 1, pp. 17–20, Jan. 2019.
[34] S. Cheng, R. Wang, J. Wu, W. Zhang, and Z. Fang, "Performance analysis and beamforming designs of mimo af relaying with hardware impairments," *IEEE Transactions on Vehicular Technology*, vol. 67, no. 7, pp. 6229–6243, Jul. 2018.
[35] A.-A. A. Boulogeorgos, N. D. Chatzidiamantis, and G. K. Karagiannidis, "Energy detection spectrum sensing under rf imperfections," *IEEE Transactions on Communications*, vol. 64, no. 7, pp. 2754–2766, Jul. 2016.
[36] S. Javed, O. Amin, S. S. Ikki, and M.-S. Alouini, "Asymmetric hardware distortions in receive diversity systems: Outage performance analysis," *IEEE Access*, vol. 5, pp. 4492–4504, Feb. 2017.
[37] S. Häfner, A. Dürr, C. Waldschmidt, and R. Thomä, "Mitigation of rf impairments of a 160-ghz mmic fmcw radar using model-based estimation," *IEEE transactions on microwave theory and techniques*, vol. 68, no. 3, pp. 1065–1073, Mar. 2019.
[38] S. Häfner, A. Dürr, R. Thomä, C. Waldschmidt, and G. Del Galdo, "High-resolution parameter estimation for chirp-sequence radar considering hardware impairments," in *2018 11th German Microwave Conference (GeMiC)*. IEEE, Mar. 2018, pp. 355–358.
[39] M. H. Moghaddam, S. R. Aghdam, A. Filippi, and T. Eriksson, "Statistical study of hardware impairments effect on mmwave 77 ghz fmcw automotive radar," in *2020 IEEE Radar Conference (RadarConf20)*. IEEE, 2020, pp. 1–6.
[40] Y. Chen, Z. Yang, J. Zhang, and M.-S. Alouini, "Further results on detection and channel estimation for hardware impaired signals," *IEEE Transactions on Communications*, vol. 69, no. 11, pp. 7167–7179, 2021.
[41] T. Schenk, *RF imperfections in high-rate wireless systems: impact and digital compensation*. Springer Science & Business Media, 2008.
[42] B. Picinbono, "Second-order complex random vectors and normal distributions," *IEEE Transactions on Signal Processing*, vol. 44, no. 10, pp. 2637–2640, 1996.
[43] A. Zaimbashi, M. Derakhtian, and A. Sheikhi, "Glrt-based cfar detection in passive bistatic radar," *IEEE Transactions on Aerospace and Electronic Systems*, vol. 49, no. 1, pp. 134–159, 2013.
[44] A. Zaimbashi, "Target detection in analog terrestrial tv-based passive radar sensor: Joint delay-doppler estimation," *IEEE Sensors Journal*, vol. 17, no. 17, pp. 5569–5580, 2017.

Junqiu Wang received the B.E. in mathematics and applied mathematics from Shandong University, Weihai, China, in 2015 and the M.E. degree in probability theory and mathematical statistics from Xiamen University, Xiamen, China, in 2019. He is currently pursuing his PhD degree for electronics engineering with the School of Engineering, University of Warwick, UK. His research interests include joint communication and radar, hardware impairment, signal processing, autonomous driving and AI for 6G.

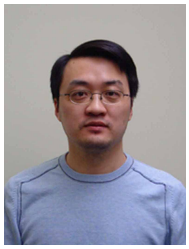

Yunfei Chen (S'02-M'06-SM'10) received his B.E. and M.E. degrees in electronics engineering from Shanghai Jiaotong University, Shanghai, P.R.China, in 1998 and 2001, respectively. He received his Ph.D. degree from the University of Alberta in 2006. He is currently working as a Professor at the University of Durham, U.K. His research interests include wireless communications, cognitive radios, wireless relaying and energy harvesting.